A Computational Framework for the Analysis of an Aero-Thermochemical-Elastic Eroding Nozzle

Eric L. Blades, Nicolas D. Reveles, Mike Nucci, and R. Scott Miskovish

ATA Engineering, Inc.

***Abstract**: A multiphysics simulation capability has been developed that incorporates mutual interactions between aerodynamics, structural response from aerothermal loading, ablation/pyrolysis, heating, and surface-to-surface radiation to perform high-fidelity, fully coupled aerothermoelastic ablation simulations, which to date had been unattainable. The multiphysics framework couples CHAR (a 3D implicit charring ablator solver), Loci/CHEM (a computational fluid dynamics solver for high-speed chemically reacting flows), and Abaqus/Standard to create a fully coupled aerothermoelastic charring ablative solver. The solvers are tightly coupled using the SIMULIA Co-Simulation Engine to resolve the effects of the ablation pyrolysis and charring process and chemistry products upon the flow field, the changes in surface geometry due to recession upon the flow field, and thermal-structural analysis of the body from the induced aerodynamic heating from the flow field. The multiphysics simulation capability was successfully demonstrated on a solid rocket motor graphite nozzle erosion application. Comparisons were made with available experimental data that measured the throat erosion during the motor firing. A series of parameter studies were conducted using the coupled simulation capability to determine the sensitivity of the nozzle erosion to different parameters. The parameter studies included the shape of the nozzle throat (flat versus rounded), material properties, the effect of the choice of turbulence model, and the inclusion/exclusion of the mechanical thermal expansion. Overall, the predicted results match the experiment very well and the predictions were able to bound the data within acceptable limits.*

***Keywords**: Ablation, Aerothermoelasticity, Co-Simulation Engine, CFD Coupling, Fluid-Structure Interaction, Multiphysics Simulation, Solid Rocket Motor, and Throat Erosion.*

1. Introduction

Aerospace systems operating in extreme thermal environments typically contain ablative components that need to be well understood to ensure mission success. In many situations, such as with thermal protection systems (TPS), the ablation is intended to both cool and protect equipment and payloads that would otherwise be damaged by high temperatures. In other cases, such as solid rocket motor (SRM) nozzles, ablation is generally not desired due to its negative impact on performance, and efforts are made to minimize the phenomenon. In SRMs, ablative materials are also used to protect the nozzle housing, and in liquid rocket engines (LREs), ablative cooling is used to provide a simple, reliable cooling method that avoids expensive and complex regenerative cooling systems requiring high-pressure pumps and tanks.

Traditionally, designs of systems and their components utilizing ablative materials have been analyzed by different engineering disciplines in an uncoupled manner, leading to a simplified superposition of independent analyses. Depending on the assumptions, this can potentially lead to overconservatism or omission of multiphysics phenomena. Analysis of such systems requires numerous simulations with various codes to numerically model the physics in the extreme environment. Effective information transfer between the domains at the physical interfaces is paramount. When these codes are loosely coupled with poorly defined interfaces, inaccuracies develop due to a lack of total system convergence.

Today's high-fidelity ablative system simulations typically include computational fluid dynamics (CFD) and an ablation response model (ARM). The CFD analyses provide heating and loading conditions, and computational structural analyses are used to ensure that the vehicle can withstand the loads. The TPS itself may require careful examination of loads caused by a coefficient of thermal expansion (CTE) mismatch at either the bondline or gap fillers (Milos, 2009). Heat transfer analyses may separately verify internal and bondline temperatures. Inaccuracies enter these simulations through many simplifications, assumptions, and uncertainties, and the simulations are frequently loosely coupled or even coupled only one way with no feedback between domain simulations (Chen 2003), (Nompelis, 2009). As such, each code solves the governing equations for the respective physical domain accurately, but at the domain boundaries the codes are not in agreement and thus will not be consistent with the actual physical problem.

A multiphysics simulation capability has been developed that incorporates mutual interactions between aerodynamics, structural response from aerothermal loading, ablation/pyrolysis, heating, and surface-to-surface radiation to perform high-fidelity, fully coupled aerothermoelastic ablation simulations, which to date had been unattainable. The multiphysics framework couples CHAR (a 3D implicit charring ablator solver), Loci/CHEM (a CFD solver for high-speed chemically reacting flows), and Abaqus/Standard to create a fully coupled aerothermoelastic charring ablative solver. The solvers are tightly coupled using the SIMULIA Co-Simulation Engine to resolve the effects of the ablation pyrolysis and charring process and chemistry products upon the flow field, the changes in surface geometry due to recession upon the flow field, and thermal-structural analysis of the body from the induced aerodynamic heating from the flow field.

The multiphysics framework addresses a unique approach to the modeling of the physics of a three-dimensional ablating surface, from the standpoint of the tight coupling of the following: the effects of the ablation pyrolysis and charring process and chemistry products upon the flow field, the changes in surface geometry due to recession upon the flow field, and thermal-structural analysis of the body from the induced aerodynamic heating from the flow field. This type of aerothermodynamic and thermal analysis problem has been a challenge for years. Typical CFD problems have been executed with fixed geometries and boundary conditions in discrete fashion, and the thermal response has been analyzed in a decoupled fashion. There have been significant advances in CFD with coupled CFD grid boundaries and unsteady solutions with potentially time-varying thermal and dynamic conditions. However, the methodology presented here takes a unique approach to the coupling of fluid, chemical, and structural dynamics of a truly time-varying solution, with chemically reacting, thermally responding, structurally changing volume and surface boundaries. This approach advances the state of the art and increases the accuracy of the predictions as all the components of the aero-thermal-elastic-ablative model are synchronized.

Validation simulations were performed using the multiphysics framework, and the validation case was taken from a series of tests whose objective was to study the nozzle erosion rates at a broad range of pressures from 7 to 34.5 MPa (1,000 to 5,000 psia) (Evans, 2010). The erosion data are well characterized, as the test rig was equipped with a windowed nozzle section for real-time X-ray radiography diagnostics of the instantaneous throat variations for deducing the instantaneous erosion rates. The nozzle initially underwent a nozzle contraction due to thermal expansion before ablation effects were able to widen the throat. These thermal effects produced deformations and stresses of significant magnitude that even resulted in the failure of the nozzle entrance piece in one of the test firings. Therefore, this case exercises all three domains of the multiphysics framework: high pressure flow of the solid motor combustion products through the nozzle (fluid domain), recession of the nozzle throat (ablator domain), and thermal expansion of the nozzle throat (structural domain).

2. Overview of the Multiphysics Framework Coupling Methodology

Rather than using a single monolithic solver, an approach that has been shown to result in numerical issues when attempting to solve the governing equations of multiple physical domains simultaneously (Guruswamy, 1992, 1993), an appropriate domain-specific solver is used for each physical domain. The multiphysics framework architecture consists of codes linked by a simulation engine that exchanges data (boundary conditions, results, geometry) between domains. The CHEM CFD code (Luke 2007) is used to solve the Navier-Stokes equations for the fluid domain and includes chemical nonequilibrium. For the ablative domain, the CHAR code (Amar, 2011) is used for the implicit charring and ablator solver, and the interface surface chemistry is coupled via the Marschall and MacLean gas-surface interaction (GSI) code (Marschall, 2011). For the structural domain, the Abaqus nonlinear structural dynamics code is used to predict the structural response. Figure 1 shows notional aerothermal ablation domains used in the multiphysics framework.

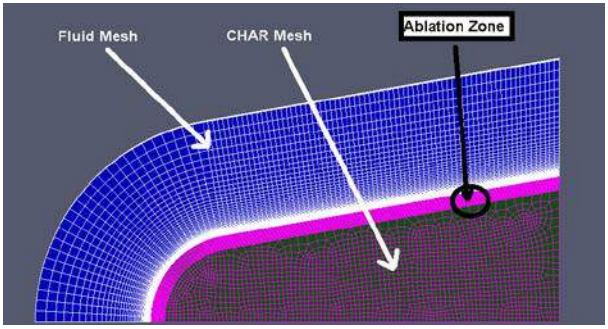

Figure 1. Discretization of fluid and ablator domains.

There are four different coupling options supported by the multiphysics framework. All utilize CHEM and CHAR for the thermochemical response, and three utilize Abaqus/Standard to compute the thermal response of the structures and, depending on the option, the mechanical response.

1. CHEM-CHAR coupling
2. CHEM-CHAR-Abaqus coupling with no mechanical degrees of freedom (DOF)
3. CHEM-CHAR-Abaqus coupling with mechanical DOF (ALE option)
4. CHEM-CHAR-Abaqus coupling with mechanical DOF (UELMAT option)

An overview of the implementation details for each of these options is provided in the following subsections.

2.1 CHEM-CHAR Coupling

The CHEM-CHAR coupling option is suitable for the class of problems that occurs where an ablative material is in contact with a fluid domain and the ablator is not intended to carry structural loads. As shown in Figure 2, the requisite boundary information is passed back and forth. In particular, heat flux, pressure, and mass fraction are passed from CHEM to CHAR, and temperature, recession rate (or displacements), and mass flux are passed from CHAR to CHEM. In addition, mass, momentum, and energy are passed between Loci/CHEM and the GSI interface.

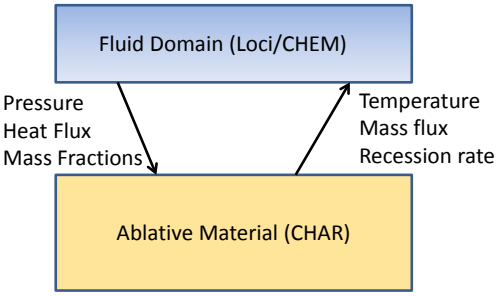

Figure 2. Information exchanged at the wetted surface between CHEM and CHAR through the CHAR API.

2.2 CHEM-CHAR-Abaqus Coupling (No Mechanical Degrees of Freedom)

The second class of problems, in which the structure is distinctly separate from the ablator, is for cases where thermal loads in the structure may be of importance or components may be temperature sensitive (e.g., ablator bond-line temperature). This coupling approach is suitable for the class of problems where the fluid, ablator, and structure are distinct, separate domains, as shown in Figure 3, and the thermal effects of the fluid on the structure are transmitted through the ablator. In this situation, the ablative material updates the heat flux to and receives temperatures from the structural domain. This approach provides a fluid/ablator/structure thermal solution where the structural thermal solution contains only thermal degrees of freedom and has no displacement within the multiphysics simulation. This approach does not provide the complete aero-thermal-chemical-mechanical solution for structures where the load-carrying structure itself is ablating.

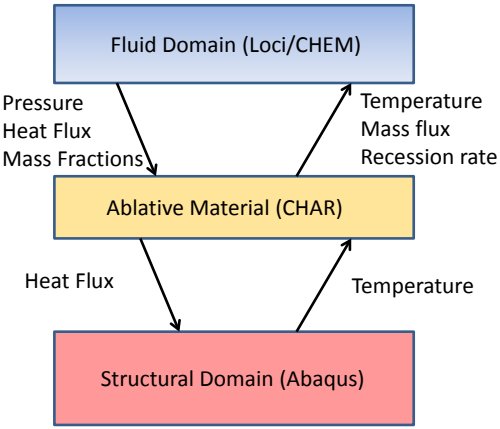

Figure 3. Information exchanged between CHEM, CHAR, and Abaqus (thermal only) through the CHAR and CSE API.

2.3 CHEM-CHAR-Abaqus Coupling (Mechanical Degrees of Freedom)

The final class of problem is when the ablative domain is carrying a structural load, i.e., an ablative hot structure, or structure is included that is attached to the ablator, e.g., the backshell attached to the heat shield. In either case, a full aero-thermal-chemical-mechanical response simulation is required, and these cases represent the most general situations where the ablated material is also a load-carrying structural member.

Since three codes are transferring information during the multiphysics simulation, the coupling is slightly more complex. With this coupling, the ablating material exists in both the ablative and structural domains, and it is required that the mesh (node locations and element topologies) be identical for the two models. CHAR computes the heat transfer, recession, and material state (virgin or charred), and Abaqus computes the deformation and stresses using temperature- and material-state-dependent properties. In addition to the information being transferred at the fluid-ablator interface between CHEM and CHAR, information is also transferred between CHEM and Abaqus to account for the mechanical response. CHEM transfers force information, including contributions due to pressure and shear stress, to Abaqus at the fluid-structure wetted surface interface, and Abaqus returns the resulting displacements. The data passed between the three codes is shown in Figure 4. The (S) indicates data passed at the surface interface between Loci/CHEM and CHAR or Abaqus, and (V) indicates volumetric data passed from CHAR to Abaqus.

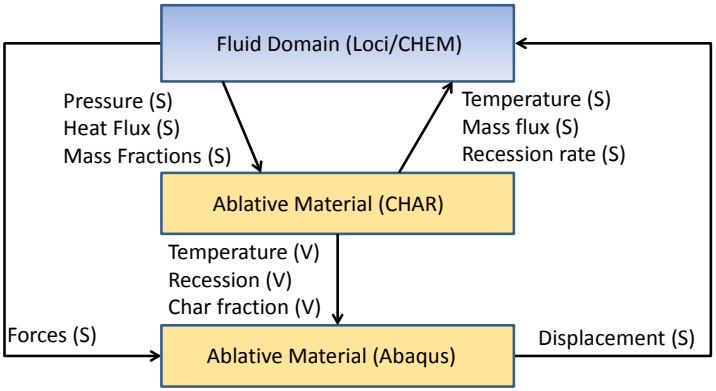

Figure 4. Information exchanged between Loci/CHEM, CHAR, and Abaqus (UMESHMOTION) through the CHAR and CSE API.

In the case where the Abaqus model includes a structural ablator model attached to a second non-ablating structural model, there is an additional coupling between CHAR and Abaqus. In this situation, the ablating mesh and non-ablating mesh require unique nodes at the interface, and these nodes should be connected together with *MPC equations that include only structural degrees of freedom; otherwise, the heat transfer will be incorrect. These *MPC equations allow the transfer of force and displacement between the two meshes. The data passed between the three codes for this option is shown in Figure 5. The (ST) indicates data passed at the surface interface between Loci/CHEM and CHAR or Abaqus, (SB) indicates data passed at the surface interface between CHAR or Abaqus and Abaqus, and (V) indicates volumetric data passed from CHAR to Abaqus.

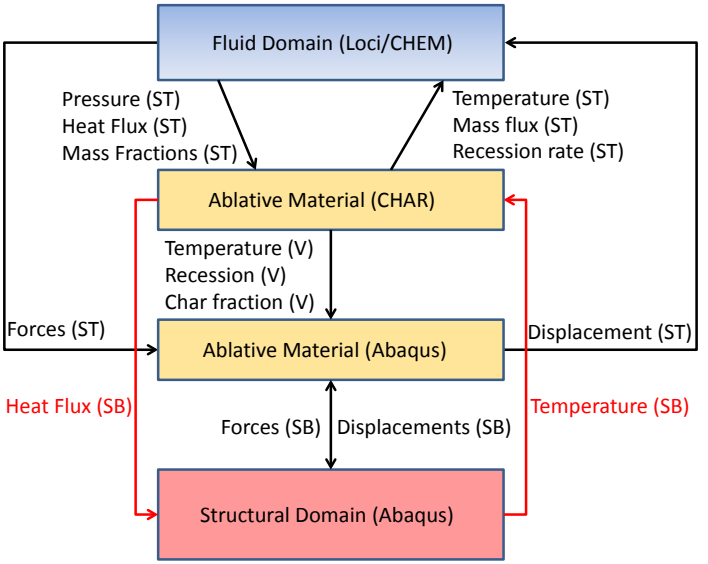

Figure 5. Data that are passed between Loci/CHEM, CHAR, and Abaqus (UMESHMOTION) through the CHAR and CSE API.

Depending on the type of mechanical analysis that is to be performed, there are two options to enforce the motion due to ablation computed by CHAR. One option uses Abaqus' Arbitrary Lagrangian-Eulerian (ALE) adaptive meshing capability and specifies the spatial mesh constraints via the UMESHMOTION user subroutine to enforce the ablative motion during adaptive meshing. The other option utilizes user-defined elements (UELs) and user material subroutines (UMATs) to enforce the motion and update the element formulation; this is referred to as the UELMAT option. The UELMAT (UEL+UMAT) approach relies on custom ablation-enabled elements, and ATA has created and verified UELMATs for linear hexahedral, pentahedral, and tetrahedral elements.

There are several differences between the ALE and UELMAT approaches. First, the ALE option is limited to quasi-static structural analyses where the kinetic energy of the structure is considered negligible, whereas the UELMAT approach offers the ability to retain the structural dynamics, i.e., the inertial and damping effects, and is therefore capable of both quasi-static and dynamic structural modeling. Second, the UELMAT approach utilizes the Co-Simulation Engine API to send the recession information, whereas the recession information for the ALE approach is communicated to the UMESHMOTION routine via file transfer. Third, the UELMAT approach can take advantage of the iterative linear equation solver within Abaqus/Standard for time-updated static solutions, which can dramatically reduce run times compared to the direct equation solver, whereas the ALE capability is limited to using the direct solver.

3. Temporal Coupling Options for the Multiphysics Framework

The various code coupling options described in the previous section can be exercised with the following temporal coupling options.

1. First-order (one data exchange per time step)
2. High-order (multiple data exchanges per time step)
3. Subcycling (multiple time steps per data exchange)

These three temporal schemes have much in common. In the developed framework, CHAR is set to lead and takes the first time step within a simulation. CHEM provides CHAR with heat flux, pressure, and local species concentrations at the wetted surface. CHAR returns to CHEM the recession, wall temperature, and change in species at the wetted surface. CHEM applies the recession to move the CFD mesh so that it is consistent with the CHAR mesh. The differences amongst these coupling schemes relate to when data exchanges occur. For simplicity, the discussion below focuses on the coupling of CHEM and CHAR, although the schemes are essentially unchanged when Abaqus is included, aside from the addition of force data that are exchanged.

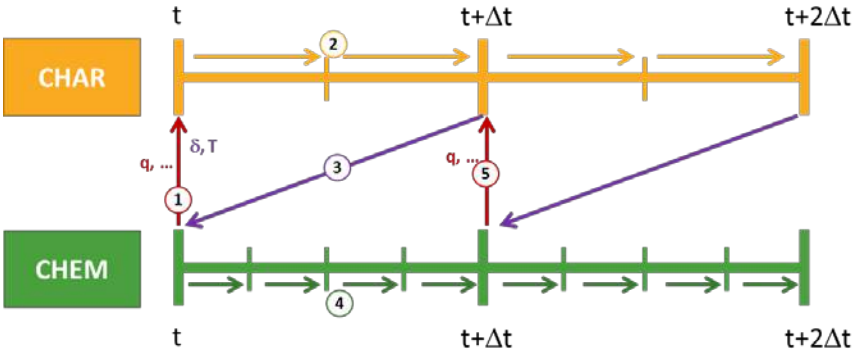

Figure 6. First-order data exchange scheme.

Figure 6 illustrates the first-order data exchange scheme. It is so named because, with sufficiently small time steps, it will ultimately reduce the temporal order of accuracy to at most first order, regardless of the temporal accuracy applied to the constituent codes. Data are exchanged after the completion of full time steps within the codes. The codes may employ unequal numbers of subiterations to get to the next time step. For this coupling scheme to work, it is essential that each code apply the same time step.

A higher-order data exchange scheme is pictured in Figure 7. This scheme applies subiteration convergence to the exchanged data to ensure that consistent data are shared between codes. This convergence removes the first-order lag error of the first-order schemes, and ultimately the order of accuracy of the coupled solution will be that of the lowest temporal accuracy of the constituent codes. As CHAR and CHEM are both at most second-order accurate, second-order temporal accuracy is the most that can be attained in this application.

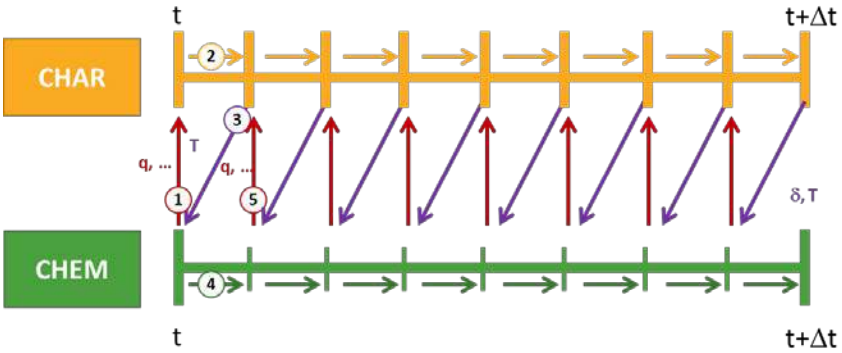

Figure 7. High-order data exchange scheme.

When considering problems with disparate time scales, it is possible to exercise a subcycling scheme, as portrayed in Figure 8. Here, the constituent codes must line up at integer values of time steps, although the number of time steps each code takes before data exchange need not be the same. For example, in the considered figure, CHEM advances four time steps and CHAR

advances just two before data are exchanged. This may be appropriate when the fluid response is much faster than the recession and the computational expense of running CHAR in lockstep with CHEM needs to be mitigated

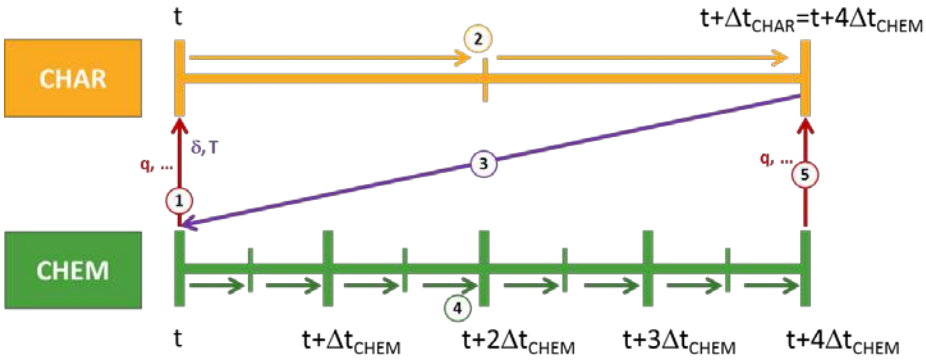

Figure 8. Subcycling coupling scheme.

4. Eroding Nozzle Validation Case

The eroding nozzle case is taken from a series of tests whose objective was to study nozzle erosion rates at a broad range of pressures from 7 to 34.5 MPa (1,000 to 5,000 psia) using two different rocket motors (Evans, 2010). The first motor, and the one of interest here, is an instrumented solid propellant motor (ISPM), which uses two baseline solid propellants: one is a nonmetallized propellant called propellant S, and the other is a metallized propellant called propellant M. The erosion data are well characterized, as the test rig was equipped with a windowed nozzle section for real-time X-ray radiography diagnostics of the instantaneous throat variations for deducing the instantaneous erosion rates. During one of the test firings, the nozzle entrance section cracked. The cracking was attributed to the thermal stress generated during the transient heating of the nozzle assembly. Additionally, the case under consideration (ISPM-07) initially underwent a nozzle contraction due to thermal expansion before ablation effects were able to widen the throat. Therefore, this case exercises all three domains of the multiphysics framework: high-pressure flow of the solid motor combustion products through the nozzle (fluid domain), recession of the nozzle throat (ablator domain), and thermal expansion of the nozzle throat (structural domain). The experimental results are readily available, and the experimental conditions are well characterized (Evans, 2009, 2010).

4.1 Computational Meshes

Multiphysics models suitable for each domain were created for the carbon nozzle case. These include the fluid dynamic meshes, boundary conditions, and constituent gas properties for the CFD solver, along with other standard inputs to the solver, and the solid mesh for both the ARM and FEM, along with standard chemical, thermal, and structural inputs to the ARM and FEM. Additional details for each of the models are provided in the following subsections. All meshes were generated from a consistent interface surface.

An unstructured 3-D viscous mesh of the nozzle, including the nozzle entrance section, was generated utilizing a structured mesh topology. A uniform spacing of 6° in the azimuthal direction was used resulting in a volume mesh size of approximately 2M hexahedral cells. It is desirable to resolve both the momentum and thermal boundary layers up to the wall, so the normal spacing of the first grid point from the wall was 1 x 10^{-5} cm, which results in a $y^+ \approx 0.1$ over the entire nozzle and is suitable for aerothermal simulations. Figure 9(a) provides an isometric view of the entire CFD mesh. Figure 9(b) illustrates a centerline through the grids used for the fluid, ablative, and structural domains. The ablation and structural domain meshes are coincident (depicted in dark green) and consist of 100,980 hexahedral elements with 108,360 nodes. The entrance piece of the CFD mesh extends beyond the solid model in order to maintain a fixed entrance area and thereby maintain the correct mass flow. As is typical and appropriate for these domains, the fluid domain has a much finer-scale resolution than the solid domain.

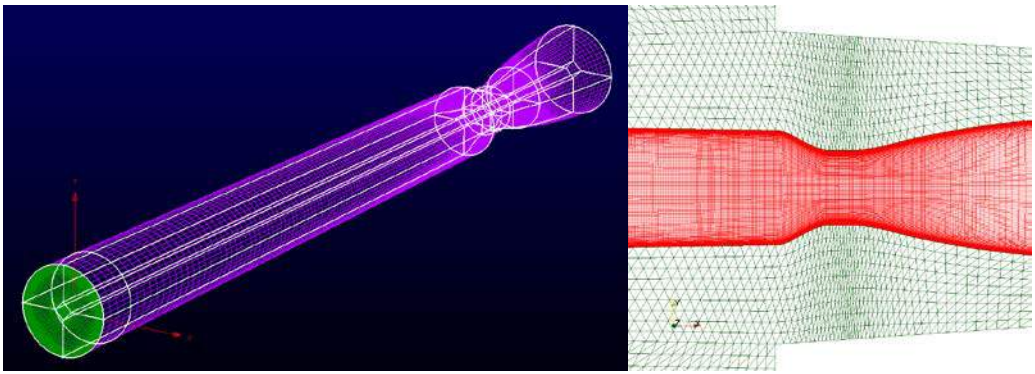

Figure 9. (a) Isometric view of the CFD mesh and (b) overlaid CFD mesh (red), and structural and ablation mesh (dark green) near the throat region.

4.2 Nozzle Properties and Operating Conditions

The nozzle is made of G-90 grade graphite, and temperature-dependent mechanical properties were used for the ARM and the FEM. For the FEM boundary conditions, the graphite nozzle was seated inside an aluminum housing that effectively pinned the exterior boundary of the nozzle.

During the experiments, metallized (aluminum oxide) and nonmetallized (ammonium perchlorate with an elastomer hydroxyl-terminated polybutadiene binder, or AP/HTPB) composite propellants were used in both motors. It was decided that the nonmetallized propellant (propellant S) would be used for simulations, since the particle size for metallized propellant was not specified and the use of the nonmetallized propellant would eliminate any mechanical erosion that might occur due to the aluminum oxide. Simulations were performed corresponding to the conditions for case ISPM-07, since this case had one of the highest erosion rates using the nonmetallized propellant and would therefore test the robustness of the multiphysics framework.

Figure 10 shows the combustion chamber pressure profile, along with the transient change in the throat diameter, for case ISPM-07. This pressure profile was digitized and used as input to the CFD transient isentropic inlet boundary condition. The digitized pressure profile (the green curve) is also included in Figure 10, overlaid for comparison to the original profile.

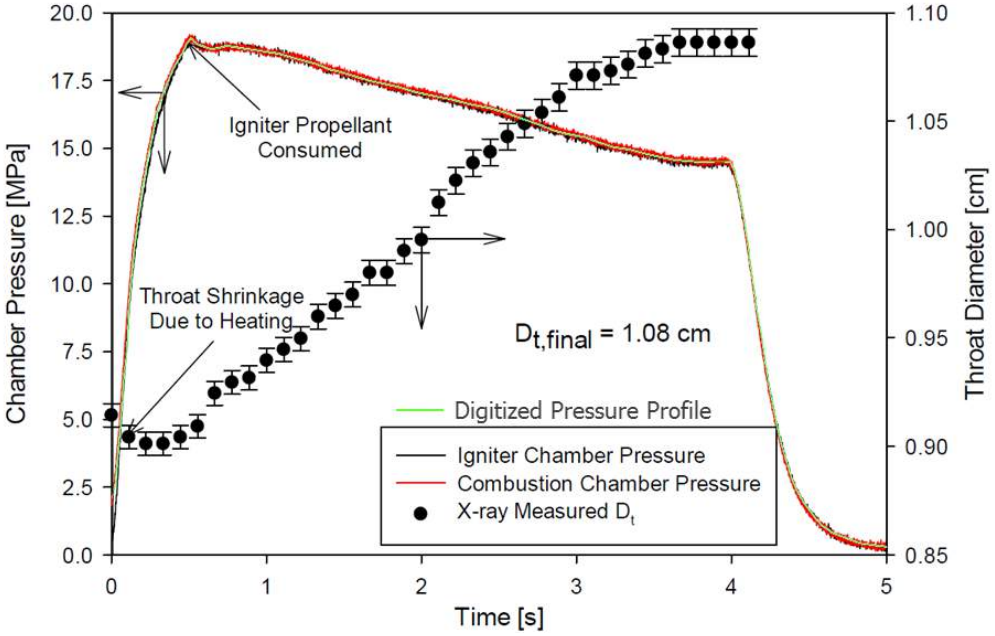

Figure 10. Combustion chamber pressure profile.

The propellant S species mass fractions for every point on the chamber pressure profile were computed using the NASA Chemical Equilibrium and Applications (CEA) program assuming ideal equilibrium chemistry (Gordon, 1994). At these conditions, there are a total of nineteen species. However, several of the species have very small mass fractions, and the number of species included in the simulation is directly proportional to the computational cost. To help reduce the computational expense, only six species were retained: H_2O, HCl, CO_2, N_2, CO, and H_2.

For all simulations, the main flow was assumed frozen and graphite nozzle ablation was assumed to be governed by the following two reactions occurring at the nozzle wall:

$$H_2O + (C) \rightarrow CO + H_2 \quad (1)$$

$$CO_2 + (C) \rightarrow 2CO \quad (2)$$

4.3 Multiphysics Simulation Parameters

For the CHEM-CHAR coupling, both codes applied a time-accurate integration scheme. The initial time step was restricted to $\Delta t = 0.0005$ s due to the large thermal gradients on the comparatively cool graphite surface encountered immediately after motor ignition. Approximately 0.1 s after motor ignition, the simulations were restarted using a time step of $\Delta t = 0.001$ s. The codes were coupled in lockstep and exchanged data six times per time step to reduce the coupling-induced error.

For the CHEM-CHAR-Abaqus coupling, CHEM and CHAR were run as previously described, and the UMESHMOTION option with Abaqus/Standard was used to perform a static analysis at

each time step to compute the mechanical response due to the pressure and shear loading from the fluid (specified by CHEM) and the temperature distribution specified by CHAR. The graphite nozzle was seated inside an aluminum housing that effectively pinned the exterior boundary of the nozzle. Due to the mechanical boundary conditions, there was not expected to be much, if any, dynamic mechanical response of the nozzle, and a static solution was assumed to be justified. This assumption was confirmed by performing an eigensolution; the natural frequency of the first mode was above 15 kHz, well above the frequency range that could be excited by the fluid dynamics.

5. Eroding Nozzle Results and Discussion

The ISPM cases began with a significant contraction of the throat diameter. This occurs due to a rapid increase in the nozzle graphite temperature causing a mechanical expansion of the graphite. As the graphite is contained in an aluminum sleeve, the graphite is constrained to expand radially inward. As the solid temperatures continue to rise, the effects of diffusion-limited ablation become nonnegligible and the nozzle diameter begins to increase due to chemical reactions physically removing material. However, as the nozzle diameter continues to grow through ablation, the effects of mechanical thermal expansion remain, and they continue to influence the ablation after they are no longer independently visible in the response.

To better resolve the interactions between the hot combustion gas and the graphite solid, a three-way coupling simulation was performed using CHEM, CHAR, and Abaqus. The addition of the mechanical model allows inclusion of the graphite thermal expansion and accounts for the effects of the internal pressure loading due to the high-pressure gas. Based on the CHEM-CHAR parameter studies (the results of which are not included here), the ablation is sensitive to a number of parameters, including turbulence model and material properties. It was anticipated that the mechanical response would be sensitive to the CTE. The manufacturer specification sheet provides different values for the CTE depending on the diameter of the graphite rod used to machine the nozzle and the smaller-diameter rod has a lower CTE than the larger-diameter rod. The diameter of the rod used to machine the nozzle was not specified, and based on the nozzle size, either could have been used. Therefore, in an attempt to bound the response, two simulations using CHEM-CHAR-Abaqus were performed. The first used the turbulence model resulting in the lowest ablation (SST) and the material model with the highest ablation rate (carbon-carbon) due to the lower conductivity and a lower CTE value. The second simulation used the BSL turbulence model with the compressibility correction, the graphite material model, and the higher CTE value. The values of the parameters used for the simulations are summarized in Table 1.

Table 1. Co-Simulation parameter summary.

Parameter	Parameter Set 1	Parameter Set 2
Turbulence model	SST	BSL
Material model	Carbon-Carbon	Graphite
CTE	Low value	High value

A comparison of the throat recession using the first set of parameters (PS1) with and without the mechanical response is shown in Figure 11. Several observations can be made regarding the inclusion mechanical response in the recession predictions. The first observation is that including the mechanical response is necessary to predicting the initial throat contraction. Figure 11(b) shows a zoomed-in view of the predicted throat recession at t = 0.0–0.5 seconds. It is obvious that there is some amount of contraction occurring when the mechanical response is included in the simulation. The calculated response from the second set of parameters (PS2) is depicted in Figure 12, and the initial contraction is much more pronounced due to the higher CTE value.

Neither case completely captures the contraction observed in the experiment; however, the presence of the throat contraction is predicted, which would not be otherwise possible if the mechanical effects were omitted. The general trends of the initial contraction are also predicted by the simulations. The PS1 simulation predicts the correct phase of the throat contraction, but the amplitude is reduced by approximately a factor of seven. The PS2 simulation approximately reproduces the amplitude, but the phase lags the experiment by half a second. It is possible that the use of a pyrogen ignitor in the experiment, which was not included in the simulations, provided a significant rise in the graphite temperature, thereby increasing the rate of contraction in a manner that the simulations were not able to reproduce.

The second observation is that without the mechanical effects, the ablation response is fairly linear (i.e., the rate of ablation is nearly constant) over the part of the pressure profile that varies linearly at t = 0.5–3.5 seconds. During this time, the ablation response without the mechanical effects tracks the pressure profile. Inclusion of the mechanical effects introduces inflections into the ablation response. As indicated in Figure 11 and Figure 12, subtle inflections are present in the nearly linear regime of the experimental data, most notably between 1.5 and 2.0 seconds.

The third observation is regarding the response toward the end the experiment. Despite significant combustion pressure and continued high temperatures, the ablation rate rolls off at approximately 3.0 seconds, essentially stopping at 3.5 seconds—well before the motor cuts off. Without the inclusion of the FEA response, it is observed that the ablation is predicted to continue unabated during this time window. When the effects of solid mechanics are included, however, a significant rolloff is observed.

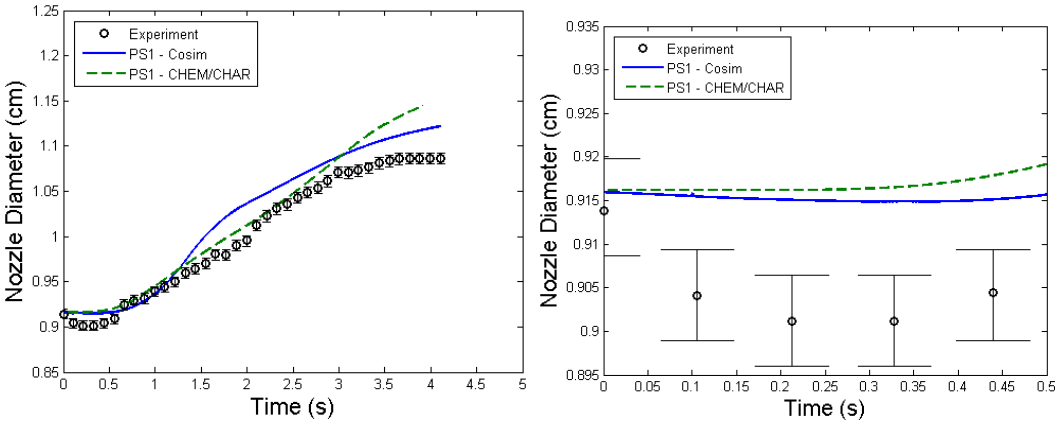

Figure 11. Throat erosion comparison with and without mechanical effects (Parameter Set 1).

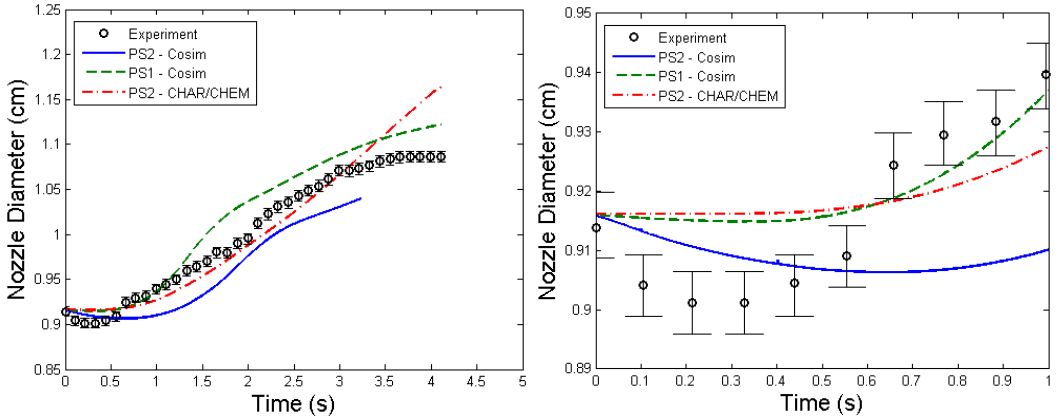

Figure 12. Throat erosion comparison with and without mechanical effects (Parameter Set 2).

Select contours and results were found for the solution corresponding to the PS2 set of parameters. Figure 13 shows a comparison of the Mach number contours in the fluid and temperature contours in the solid at two different times during the simulation: at t = 0.5 s and t = 4.1 s. At t = 0.5 s, very little erosion of the throat has occurred, whereas the throat has eroded significantly at t = 4.1 s. The fluid in the expansion part of the nozzle has reduced velocity at t = 4.1 s (Figure 13b) as compared to t = 0.5 s (Figure 13a) due to the increase in the throat area, and it is this decrease in the flow speed that is responsible for the performance loss of the motor. Also, a different shock structure has set up in the eroded nozzle as compared to the nozzle at t = 0.5 s. As expected, the temperature in the solid domain is appreciable hotter, nearly 1000 K hotter at the nozzle wall, at t = 4.1 s than at t = 0.5 s. Away from the nozzle, the temperature is also hotter throughout the solid domain at t = 4.1 s than at t = 0.5 s.

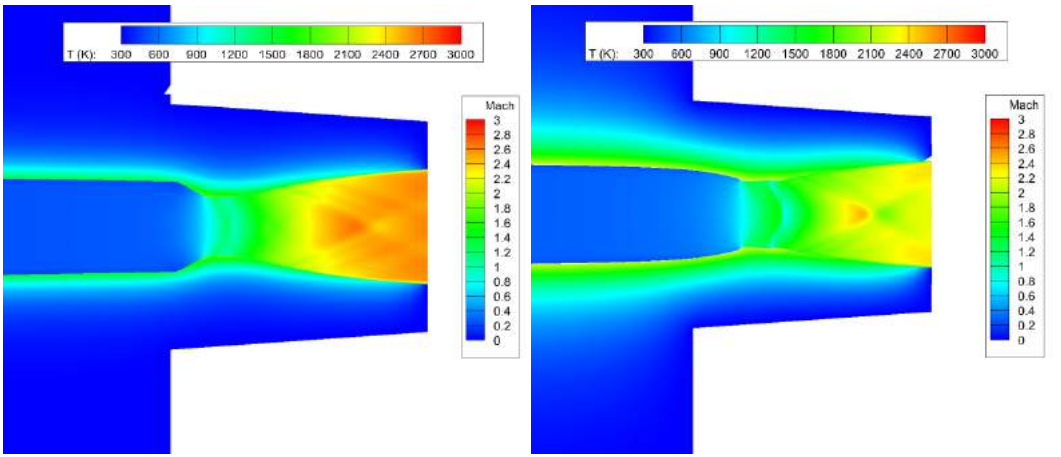

Figure 13. Mach number (fluid) and temperature (solid) contours at (a) t = 0.5 s and (b) t = 4.1 s.

A comparison of the initial and eroded throat profile from one of the simulations is shown in Figure 14, illustrating how much the throat area has increased. Note that the converging section of the eroded throat profile has changed significantly, and there is no longer a flat section at the throat. Unfortunately, no experimental data were available for comparison of the eroded throat profile.

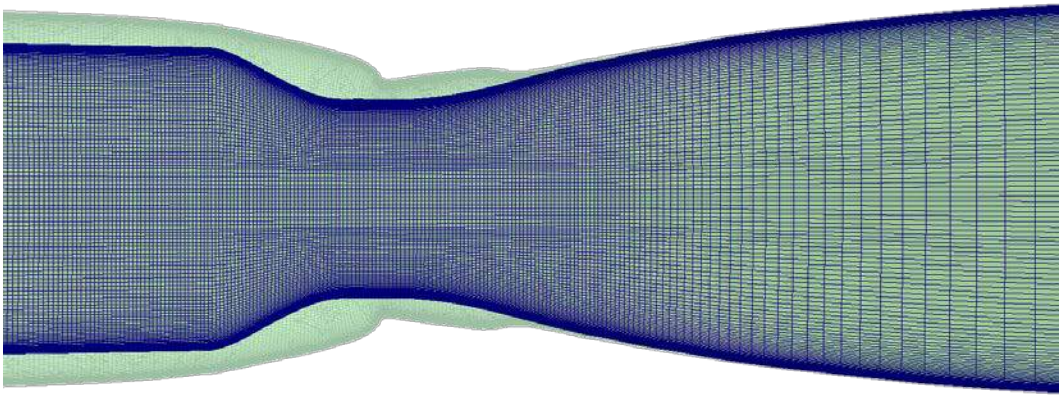

Figure 14. Comparison of the initial nozzle profile (blue) and the eroded nozzle profile (light green).

6. References

1. Milos, F.S., and Y.-K. Chen, "Ablation and Thermal Response Property Model Validation for Phenolic Impregnated Carbon Ablator," AIAA-2008-0262, 2009.

2. Chen, Y.-K., et al., “Graphite Ablation and Thermal Response Simulation Under Arc-Jet Flow Conditions,” AIAA-2003-4042, 2003.
3. Nompelis, I., G. Candler, and R. Conti, “A Parallel Implicit CFD Code for the Simulation of Ablating Re-Entry Vehicles,” AIAA-2009-1562, January 2009.
4. Evans, B, “Nozzle Erosion Characterization and Minimization for High-Pressure Rocket Motor Applications,” Ph.D. dissertation, Pennsylvania State University, 2010.
5. Evans, B., K.K. Kuo, E. Boyd, and A.C. Cortopassi, “Comparison of Nozzle Throat Erosion Behavior in a Solid-Propellant Rocket Motor and a Simulator,” AIAA-2009-5421, 2009.
6. Guruswamy, G.P., “Coupled Finite-Difference/Finite Element Approach for Wing-Body Aeroelasticity,” AIAA-1992-4680-CP, 1992.
7. Guruswamy, G.P, and C. Byun., “Fluid-Structural Interactions using the Navier-Stokes Flow Equations Coupled with Shell Finite Element Structures,” AIAA-1993-3087, 1993.
8. Luke, E, “On Robust and Accurate Arbitrary Polytope CFD Solvers (Invited),” AIAA 2007-3956. AIAA Computational Fluid Dynamics Conference, 2007.
9. Amar, A., N. Calvert, and B. Kirk, “Development and Verification of the Charring Ablating Thermal Protection Implicit System Solver,” AIAA-2011-0144, 2011.
10. Marschall, J., and M. MacLean, “Finite-Rate Surface Chemistry Model, Part I,” AIAA-2011-3783, 2011.
11. Gordon, S., and B.J. McBride, “Computer Program for Calculation of Complex Chemical Equilibrium Compositions and Applications,” NASA RP-1311, 1994.

7. Acknowledgements

This work was done under SBIR funding from the NASA Marshall Space Flight Center, contract NNX16CM45P, Mr. Brandon Mobley, program manager. This support is gratefully acknowledged.